ELSEVIER

Composites Science and Technology 60 (2000) 2097–2106

COMPOSITES SCIENCE AND TECHNOLOGY

www.elsevier.com/locate/compscitech

Integrated thermal and mechanical analysis of composite plates and shells

R. Rolfes, K. Rohwer *

DLR, Institute of Structural Mechanics, PO Box 3267, D-38022 Braunschweig, Germany

Received 17 August 1999; accepted 11 May 2000

Abstract

Thermal and mechanical analyses of structures are usually performed with non-consistent tools leading to an excessive effort in data adaptation. The application of 2D finite elements for both tasks relaxes this deficiency. With thermal lamination theories assuming a linear or quadratic temperature distribution in the thickness direction, suitable elements are developed and experimentally verified for both steady-state and transient problems. On the basis of a 2D global analysis accurate transverse stresses can be determined from local equilibrium conditions. For laminated plates and cylindrical shells a procedure is presented which allows us to reduce the order of shape functions. © 2000 Elsevier Science Ltd. All rights reserved.

Keywords: A. Layered structures; B. Thermomechanical properties; C. Finite element analysis (FEA); C. Laminate theory

1. Motivation and introduction

Cost reduction, increased damage tolerance and improved failure prediction will be key issues for widening the application of composite materials. On the one hand, new fabrication technologies based on dry-fibre preforms and resin injection promise a big potential for cost reduction, and, on the other hand, the whole development chain for composite structures ranging from design over analysis to fabrication and qualification can be made much more efficient by providing an integrated development environment. Major elements of such an environment are analysis tools integrating all analysis disciplines which are necessary for safe and economic design and layout of composite structures. The present paper focuses on modern aerospace structures under simultaneous thermal and mechanical loading, e.g. composite airframe structures for the next generation of commercial airliners when exposed to high levels of solar irradiation, large orbital structures under thermal cycling, the load-carrying structures of future reusable launchers or advanced ceramic propulsion components. The major disciplines involved are thermal and stress analysis. This paper presents finite-element methods which provide the full 3D temperature and stress fields based on a shell representation of the composite structure only. The 3D stress field is of special importance with respect to failure prediction, since transverse stresses, which are usually neglected, can very much influence both the onset and growth of delaminations and failure under compressive loads transverse to the fibres. Consequently, advanced failure criteria for composites [6,10,21]) account for the three-dimensional (3D) state of stress.

2. Thermal analysis

2.1. State of the art in 3D thermal analysis

Most composite materials are thermally anisotropic and inhomogeneous since the conductivities of fibres and matrix differ significantly. This must be taken into account if accurate results are to be achieved.

Padovan [19] has therefore proposed a layerwise discretisation with 3D elements, which is very costly. The effort can be reduced by modelling a couple of layers with only one 3D element [37]. However, the influence of the stacking sequence within one element is ignored. 2D elements for axisymmetric problems with variable polynomial degree of the shape functions in both the longitudinal and radial directions [3,36]) are capable of describing the pronounced non-linear transverse temperature distribution which occurs in extremely thick-walled cylindrical structures.

*Corresponding author. Tel.: +49-531-295-2384; fax: +49-531-295-2875.

E-mail address: klaus.rohwer@dlr.de (K. Rohwer).

PII: S0266-3538(00)00117-2

In thin-walled to moderately thick-walled structures, the transverse temperature distribution can be approximated by a linear or quadratic function. This is the basic assumption of thermal laminate theories (TLT) for composite structures [27–29]. They allow for the setting up of 2D finite elements capable of describing the full 3D heat conduction problem. A linear temperature distribution as assumed by the linear TLT provides good results for steady state and transient problems. Under extremely concentrated loads and during the initial phase of transient processes, a quadratic temperature distribution is more suitable. Very good performance of the quadratic TLT and the related finite-element analysis has been shown for linear and non-linear problems.

Noor and Burton [15] have proposed a predictor/corrector approach where they have applied the linear TLT in the predictor phase; in the corrector phase they have used the 3D heat-conduction equation and the constitutive law in order to improve the linear temperature distribution in thickness direction. Argyris et al. [2], and Argyris and Tenek [1] have used the linear TLT in conjunction with triangular elements for solving steady-state problems with non-linearities caused by radiative boundary conditions and temperature-dependent conductivities. Subsequently, a short description of the TLT is given and related finite shell elements are presented together with applications to non-linear problems and experimental verifications.

2.2. Development of computational strategy

On the conditions

- that the thermal conductivity in the thickness direction is identical for all layers, and
- that there is no heat-transfer resistance at the interfaces,

the temperature distribution in the thickness direction of a laminated composite plate can in many cases be expressed by a linear function. This is the fundamental assumption of the linear TLT. It can be formulated as

$$T(x_1, x_2, x_3) = T^{(0)}(x_1, x_2) + T^{(1)}(x_1, x_2)\cdot x_3 \tag{1}$$

where $T^{(0)}$ and $T^{(1)}$ are the temperature and the gradient in thickness direction of the reference plane, respectively. x_1 and x_2 are the in-plane coordinates while x_3 denotes the thickness direction. Non-linear temperature distributions in the thickness direction can occur in cases of

- large temperature gradients in the thickness direction in conjunction with temperature-dependent thermo-physical properties.
- transient problems with rapid heating
- spatially concentrated thermal loads.

In such cases, the quadratic TLT is better suited. It assumes

$$T(x_1, x_2, x_3) = T^{(0)}(x_1, x_2) + T^{(1)}(x_1, x_2)\cdot x_3 + \tfrac{1}{2}\cdot T^{(2)}(x_1, x_2)\cdot x_3^2, , \tag{2}$$

which can be expressed in matrix form as

$$T = \underline{X}_{\mathrm{QL}}\underline{\rho}_{\mathrm{QL}}, \tag{3}$$

where

$$\underline{X}_{\mathrm{QL}} = \begin{bmatrix} 1 & 0 & 0 & x_3 & 0 & 0 & \tfrac{1}{2}x_3^2 & 0 & 0 \end{bmatrix} \tag{4}$$

comprises the approximation function in thickness direction and

$$\underline{\rho}_{\mathrm{QL}} = \left\{ T^{(0)}\ T^{(0)}_{,1}\ T^{(0)}_{,2}\ T^{(1)}\ T^{(1)}_{,1}\ T^{(1)}_{,2}\ T^{(2)}\ T^{(2)}_{,1}\ T^{(2)}_{,2} \right\} \tag{5}$$

is the vector of functional degrees of freedom. Given this, the gradient can be written as

$$\mathrm{grad}\,T = \underline{Y}_{\mathrm{QL}}\underline{\rho}_{\mathrm{QL}} \tag{6}$$

with

$$\underline{Y}_{\mathrm{QL}} = \begin{bmatrix} 0 & 1 & 0 & 0 & x_3 & 0 & 0 & \tfrac{1}{2}x_3^2 & 0 \\ 0 & 0 & 1 & 0 & 0 & x_3 & 0 & 0 & \tfrac{1}{2}x_3^2 \\ 0 & 0 & 0 & 1 & 0 & 0 & x_3 & 0 & 0 \end{bmatrix}. \tag{7}$$

The index 'QL' points to the quadratic TLT. When introducing this approach into Fourier's law of heat conduction

$$q = -\underline{\tilde{K}}\cdot\mathrm{grad}\,T \tag{8}$$

it follows

$$\underline{q} = -\underline{\tilde{K}}\,\underline{Y}_{\mathrm{QL}}\underline{\rho}_{\mathrm{QL}}\cdot \tag{9}$$

$\underline{q}$ denotes the heat flux vector and $\underline{\tilde{K}}$ is the rank-2-tensor of the thermal conductivity of a unidirectional lamina with monoclinic symmetry. Multiplying Eq. (9) with $\underline{Y}^{\mathrm{T}}_{\mathrm{QL}}$ from the left side and integrating over the thickness provides the quadratic law of heat conduction of the laminate

$$\underline{\hat{Q}}_{\mathrm{QL}} = -\underline{\hat{K}}_{\mathrm{QL}}\underline{\rho}_{\mathrm{QL}}\cdot \tag{10}$$

where

$$\underline{\hat{K}}_{\mathrm{QL}} = \int_h \underline{Y}^{\mathrm{T}}_{\mathrm{QL}}\underline{\hat{K}}\,\underline{Y}_{\mathrm{QL}}\mathrm{d}x_3 \tag{11}$$

is the quadratic matrix of heat conduction of the laminate. Writing Eq. (10) in component form gives

$$\begin{bmatrix} 0 \\ \hat{Q}_1 \\ \hat{Q}_2 \\ \hat{Q}_3 \\ \hat{M}_1^{(q)} \\ \hat{M}_2^{(q)} \\ \hat{M}_3^{(q)} \\ {}^2\hat{M}_1^{(q)} \\ {}^2\hat{M}_2^{(q)} \end{bmatrix} = -$$

$$\begin{bmatrix} 0 & 0 & 0 & 0 & 0 & 0 & 0 & 0 & 0 \\ & A_{11}^{(q)} & A_{12}^{(q)} & 0 & B_{11}^{(q)} & B_{12}^{(q)} & 0 & \frac{1}{2}D_{11}^{(q)} & \frac{1}{2}D_{12}^{(q)} \\ & & A_{22}^{(q)} & 0 & B_{12}^{(q)} & B_{22}^{(q)} & 0 & \frac{1}{2}D_{12}^{(q)} & \frac{1}{2}D_{22}^{(q)} \\ & & & A_{33}^{(q)} & 0 & 0 & B_{33}^{(q)} & 0 & 0 \\ & & & & D_{11}^{(q)} & D_{12}^{(q)} & 0 & \frac{1}{2}E_{11}^{(q)} & \frac{1}{2}E_{12}^{(q)} \\ & & \text{sym.} & & & D_{22}^{(q)} & 0 & \frac{1}{2}E_{12}^{(q)} & \frac{1}{2}E_{22}^{(q)} \\ & & & & & & D_{33}^{(q)} & 0 & 0 \\ & & & & & & & \frac{1}{4}F_{11}^{(q)} & \frac{1}{4}F_{12}^{(q)} \\ & & & & & & & & \frac{1}{4}F_{22}^{(q)} \end{bmatrix}$$

$$\begin{bmatrix} T^{(0)} \\ T_{,1}^{(0)} \\ T_{,2}^{(0)} \\ T^{(1)} \\ T_{,1}^{(1)} \\ T_{,2}^{(1)} \\ T^{(2)} \\ T_{,1}^{(2)} \\ T_{,2}^{(2)} \end{bmatrix}, \tag{12}$$

where the coefficients of the heat conduction matrix of the laminate read as follows

$$A_{ij}^{(q)} = \sum_{k=1}^{k} k_{ij}^{(k)} h_k \qquad B_{ij}^{(q)} = \frac{1}{2}\sum_{k=1}^{n} k_{ij}^{(k)} \left(\left(x_3^{(k+1)}\right)^2 - \left(x_3^{(k)}\right)^2 \right)$$

$$D_{ij}^{(q)} = \frac{1}{3}\sum_{k=1}^{n} k_{ij}^{(k)} \left(\left(x_3^{(k+1)}\right)^3 - \left(x_3^{(k)}\right)^3 \right)$$

$$E_{ij}^{(q)} = \frac{1}{4}\sum_{k=1}^{n} k_{ij}^{(k)} \left(\left(x_3^{(k+1)}\right)^4 - \left(x_3^{(k)}\right)^4 \right)$$

$$F_{ij}^{(q)} = \frac{1}{5}\sum_{k=1}^{n} k_{ij}^{(k)} \left(\left(x_3^{(k+1)}\right)^5 - \left(x_3^{(k)}\right)^5 \right) \tag{13}$$

$\hat{Q}_i$ are the heat flux resultants, and $\hat{M}_i^{(q)}$ and ${}^{(2)}\hat{M}_i^{(q)}$ are first- and second order heat flux moments, respectively. They appear as

$$\begin{bmatrix} \hat{Q}_i \\ \hat{M}_i^{(q)} \\ {}^{(2)}\hat{M}_i^{(q)} \end{bmatrix} = \int_h q_i \begin{bmatrix} 1 \\ x_3 \\ x_3^2 \end{bmatrix} \mathrm{d}x_3. \tag{14}$$

It should be pointed out that $\hat{Q}_3$ and $\hat{M}_3^{(q)}$ are always decoupled from the in-plane coordinates x_1 and x_2, which is a result of the monoclinic symmetry of the individual layers. However, the theory can also account for non-monoclinic laminates, e.g. with fibres that are not parallel to the middle surface of the layers (stitched multi-axial laminates). There are merely additional coupling terms to be accounted for.

The index 'QL' is hereafter omitted, indicating that either of the TLTs can be applied. Both theories can be favourably used for constructing special finite elements. The starting point is the weak form of the general heat conduction equation

$$\int_\Omega \mathrm{div}\left(\underline{\tilde{K}}\ \mathrm{grad}\ T\right) v\,\mathrm{d}\omega = \int_\Omega \rho c \dot{T} v \mathrm{d}\omega, \tag{15}$$

where ρ and c denote density and specific heat capacity of the composite material, ω is the domain in $\mathcal{R}^3$, and v stands for the test functions. Boundary conditions are specified as

$$T = \overline{T} \text{ on } \Gamma_1 \tag{16}$$

and

$$\underline{q}^T \underline{n} - q_c - \overline{q} = 0 \text{ on } \Gamma_2 \tag{17}$$

$\bar{T}$ and $\bar{q}$ are prescribed temperature and heat flux, respectively, $\underline{n}$ is the outward normal vector at the boundary Γ_2, and q_c describes convective heat exchange as

$$q_\mathrm{c} = h_c(T - T_\mathrm{ak}). \tag{18}$$

h_c denotes the convection coefficient and T_ak is the ambient temperature. Eq. (17) does not take into account radiation boundary conditions. They will be added after having derived the system of finite-element equations. Applying Green's law to Eq. (15) allows for shifting one order of differentiation from the unknown variable T to the test functions:

$$-\int_\Omega (\mathrm{grad}\, v)^T \underline{\tilde{K}}\ \mathrm{grad} T\ \mathrm{d}\omega + \int_{\Gamma_2} \left(\underline{\tilde{K}} \mathrm{grad} T\right)^T \underline{n}\ v\ \mathrm{d}\gamma = \int \rho\ c\ \dot{T}\ v\ \mathrm{d}\omega. \tag{19}$$

Introducing Eqs. (3) and (6) and splitting the domain according to

$$\mathrm{d}\omega = \mathrm{d}a\cdot\mathrm{d}x_3 \tag{20}$$

yields

$$\int_A \underline{\chi}^T \underline{\hat{K}}\underline{\rho}\, da + \int_{\Gamma_2} h_c \underline{\chi}^T \underline{X}^T \underline{X}\underline{\rho}\, \mathrm{d}s + \int_A \underline{\chi}^T \underline{\hat{C}}\underline{\dot{\rho}}\, \mathrm{d}a = \int_{\Gamma_2} (h_c T_{ak} - \bar{q})\underline{\chi}^T \underline{X}^T \mathrm{d}s, \tag{21}$$

where $\underline{\chi}$ comprises the functional degrees of freedom of the test functions and $\underline{\hat{C}}$ is the heat capacity matrix of the laminate

$$\underline{\hat{C}} = \rho c \int_h \underline{X}^T \underline{X} \mathrm{d}x_3. \tag{22}$$

A simple discretisation using quadrilateral elements and bilinear shape functions leads to a conforming finite-element approximation. It is expressed by

$$\underline{\rho} = \underline{\underline{N}}\,\underline{\vartheta}, \tag{23}$$

where $\underline{\underline{N}}$ comprises the shape functions and $\underline{\vartheta}$ is the vector of nodal degrees of freedom. $\underline{\vartheta}$ contains eight components for the linear TLT and 12 for the quadratic theory. The related finite elements are denoted QUADTL and QUADQL. Inserting Eq. (23) into Eq. (21) finally leads to the finite-element equation system

$$\underline{K}\underline{\Theta} + \underline{C}\underline{\dot{\Theta}} = \underline{Q}, \tag{24}$$

where $\underline{\Theta}$ is the global vector of unknowns, $\underline{Q}$ is the finite-element thermal load vector, and $\underline{K}$ and $\underline{C}$ denote the finite element conduction and capacity matrix, respectively. They appear as

$$\underline{K} = \sum_{i=1}^{n_e} \left(\int_{A_i} \underline{\underline{N}}^T \underline{\hat{K}}\, \underline{\underline{N}}\, \mathrm{d}a + h_c \int_{\Gamma_{2i}} \underline{\underline{N}}^T \underline{X}^T \underline{X}\, \underline{\underline{N}}\, \mathrm{d}s \right), \tag{25}$$

$$\underline{C} = \sum_{i=1}^{n_e} \left(\int_{A_i} \underline{\underline{N}}^T \underline{\hat{C}}\, \underline{\underline{N}} \mathrm{d}a \right), \tag{26}$$

$$\underline{Q} = \sum_{i=1}^{n_e} (h_c T_{ak} - \bar{q}) \int_{\Gamma_{2i}} \underline{\underline{N}}^T \underline{X}^T \mathrm{d}s. \tag{27}$$

Radiation exchange can be taken into account by adding the radiation load vector

$$\underline{Q}_s = \underline{T}^T \underline{S}_A\, \underline{T}\, \underline{\Theta}^4 \tag{28}$$

to the right-hand side of Eq. (24), where $\underline{S}_A$ is the radiation exchange matrix and T is a matrix for transforming the radiative load from the elements to the nodal points. That is required since $\underline{S}_A$ is defined between elements according to

$$\underline{S}_A = \sigma_{SB} \left(\underline{I} - \underline{\underline{F}} \right) \underline{\underline{A}}\, \underline{\underline{\varepsilon}} \left(\underline{I} - \underline{\underline{F}} \left(\underline{I} - \underline{\underline{\varepsilon}} \right) \right)^{-1}, \tag{29}$$

where σ_{SB} is the Stefan–Boltzmann-constant. $\underline{\underline{A}}$ and $\underline{\underline{\varepsilon}}$ are diagonal matrices of the element area and emissivities. $\underline{\underline{F}}$ is the symmetric view factor matrix the evaluation of which is usually very time consuming. This, together with the strong non-linearity [cf. Eq. (28)] makes radiative boundary conditions very costly. Additional non-linearities can occur as a consequence of the temperature dependence of the thermo-physical properties.

2.3. Numerical examples

The performance of the finite elements QUADTL and QUADQL for non-linear problems is demonstrated by two examples. The first is a skin-stringer configuration with stacking sequences $[0_4|45_3|0_4|{-}45_3|0_4|90_2]_{sym}$ for the skin and $[0_2|45|0_2|{-}45_2|0|90]_{sym}$ for the stringer. It is exposed to a concentrated heat flux of 20 kW/m^2. There are adiabatic boundary conditions on the upper side of the skin and convection with $h_c = 30$ W/m^2 K on the lower side and on both sides of the stringer. Non-linearity is caused by the temperature-dependent thermo-physical properties which are given in Table 1.

Fig. 1 shows steady-state temperature distributions on the upper side of the skin calculated by QUADTL, QUADQL and MSC/NASTRAN. The NASTRAN results were achieved by using a 3D model with one

Table 1
Thermo-physical properties of M50/epoxy

T (°C)	k_1(W/mK)	k_2 (W/mK)	c (J/gK)	ρ (g/cm^3)
30	54.0	0.96	0.84	1.66
120	86.4	1.06	1.09	1.66

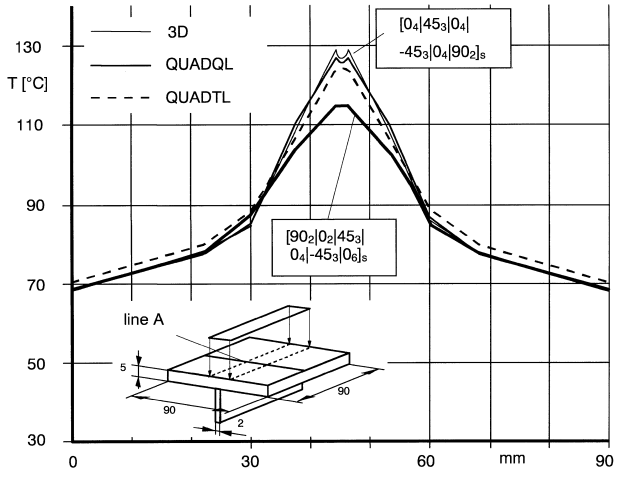

Fig. 1. Comparison of QUADTL and QUADQL with 3D results (non-linear analysis).

HEXA element per layer. This results in a computing time which is 30 to 60 times greater, as compared to QUADQL or QUADTL, respectively. Nevertheless, the approximation of the QUADTL and QUADQL results to the 3D solution is very good. A slight change of the stacking sequence of the skin to $[90_2|0_2|45_3|0_4|-45_3|0_6]_{sym}$ has a significant influence on the peak temperature which is very well reflected by both of the elements (thick solid line in Fig. 1).

The representation of radiative boundary conditions is tested by the example of a two-layered plate ($[+45|-45]$, $k_1 = 30$ W/mK, $k_2 = 1.1$ W/mK) subjected to a heat flux of 500 W/m^2. Radiation with $\varepsilon = 0.9$ is assumed on the upper side of the plate, whereas convection with $h_c = 30$ W/m^2 K acts on the lower side. Fig. 2 shows QUADTL and 3D-MSC/NASTRAN results. The overall agreement is excellent, only a small deviation occurring at the bottom side directly underneath the load.

2.4. Experimental verification

Experimental investigations were carried out in order to verify the results of the elements QUADTL and QUADQL. Heating up a plate uniformly from one side would have been rather simple. However, such a loading condition would cause a 1D transverse heat flow through the plate which is not affected by the stacking sequence. However, the stacking has a big influence in the case of 3D heat flow which occurs, for example, in structures like that depicted in Fig. 1. Thus, three geometrically identical T-shaped test structures differing only in the stacking sequences were selected. Furthermore, an extremely anisotropic CFRP material with $k_1/k_2 = 295$ (at room temperature and for 0.65 fiber-volume fraction) was chosen.

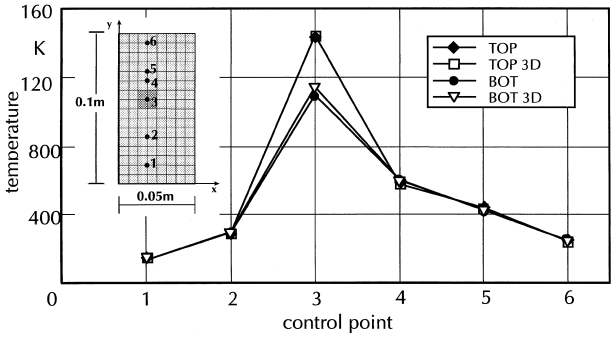

Fig. 2. Representation of radiative boundary conditions.

The temperature fields of the three test structures differ the more, the higher the temperature gradients are within the structures. Therefore, tests with cooling the stiffener by liquid nitrogen were carried out leading to a temperature difference of more than 300°C within the structure. Such extreme conditions can arise in a future launch vehicle with a hot outer skin and cryogenic fuel inside. However, realistic thermophysical data for the cryogenic temperature range were not available. They had to be estimated so that only a qualitative comparison between tests and calculation was possible. Additionally, tests with conventional air cooling were conducted. The effects were much smaller, but a qualitative comparison of tests and calculations was feasible.

Fig. 3 shows a bottom and a top view of one of the T-shaped test structures. The wires of the thermocouples (type K, DIN IEC 584) can be clearly seen. The sampling points are located at the ends of the wires in the symmetry plane of the test structure. The thermocouples are concentrated near the root of the stiffener, where the highest temperature gradients were expected. By that means, the temperature distributions along lines A and B (cf. Fig. 4) could be accurately recorded. Table 2 lists the thermo-physical properties. While the conductivity of the matrix and the specific heat capacity were measured, the conductivities of the fibre were provided by the

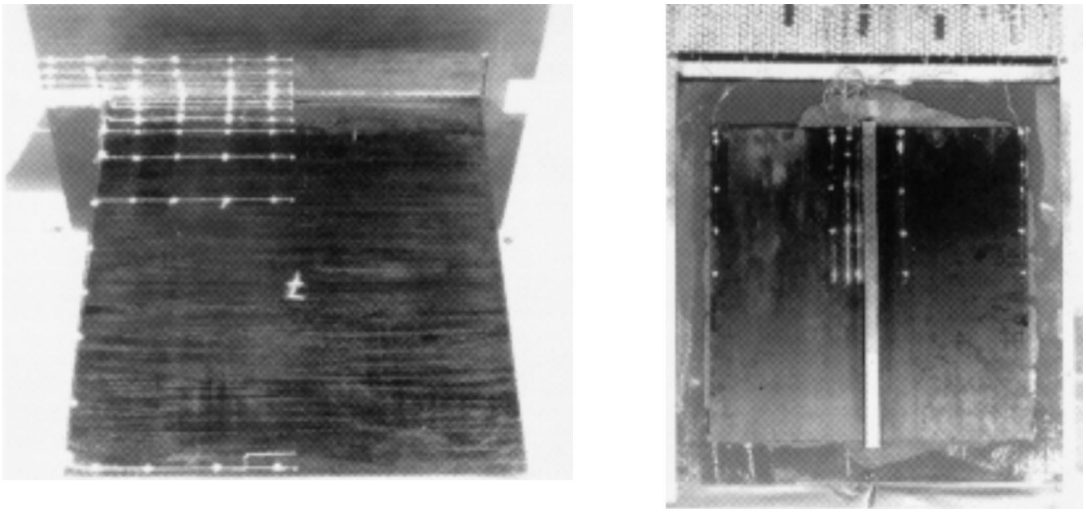

Fig. 3. CFRP test structure with thermocouples.

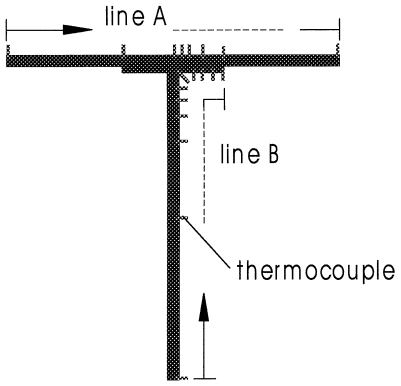

Fig. 4. Position of temperature sampling points.

Table 2
Thermo-physical properties of FT700/LY556

T (°C)	k_f^{II} (W/mK)	$k_f^{\perp}$(W/mK)	k_m (W/mK)	c_p (J/gK)
RT	345	2.4		0.85
30			0.23	
100	361			
120			0.23	1.12
150		2.9		

manufacturer. The thermal conductivities of a unidirectional layer are needed as input data for the finite-element calculation. The conductivity in the fibre direction, k_1, was calculated from the rule of mixtures, the conductivity perpendicular to the fibres, k_2, was determined by use of the self-consistent formula recently qualified [30]. Since no thermo-physical data of FT700/LY556 were available for the cryogenic temperature range, measurements on an M40A/epoxy specimen [9] were used. Derived from those are the temperature coefficients given in Table 3. However, since the FT700 fibre is much stiffer than the M40A fibre, the applicability of the coefficients is still to be proved. Three test structures were fabricated, the stacking sequences of which are quoted in Table 4 and schematically depicted in Fig. 5. Only the sequence, but not the number of 0°, ±45°, 90° layers, was changed in order to show the influence of the stacking sequence on the temperature field.

The test set-ups with air and liquid nitrogen cooling are shown in Fig. 6. In both cases the heat was introduced along a line in stiffener direction (0° direction) by an infrared radiator lamp. The remaining upper surface of the structure was covered with insulation material. The boundary conditions on the lower side were convection in the case of air cooling, and adiabatic and constant temperature in the case of liquid-nitrogen cooling. The ribs improved the efficiency of the liquid-nitrogen cooling.

At the beginning of the tests with air cooling, the test structures were at room temperature (isothermal). In the case of liquid-nitrogen cooling, no isothermal state was

Table 3
Temperature coefficients of FT700/LY556

T (°C)	$\alpha_{k_{11}}$	$\alpha_{k_{\perp}}$	α_{c_p}
150	–	1.06	–
130	1.06	–	–
120	–	–	1.32
RT	1	1	1
−73	0.90	0.94	0.74
−123	0.70	0.72	0.59
−173	0.33	0.38	0.42
−213	0.067	0.16	0.27

Table 4
Stacking sequences of test structures

Structure	Skin/stiffener	Stacking sequence
HS0/0	Skin H0	$[0_7/+45/-45/90_7/+45]_s$
	Stiffener S0	$[0_{13}/(+45/-45)_2/90_{13}]_s$
HS0/90	Skin H0	See above
	Stiffener S90	$[90_{13}/(-45/+45)_2/0_{13}]_s$
HS90/90	Skin H90	$[90_7/+45/-45/0_7/+45]_s$
	Stiffener S90	See above

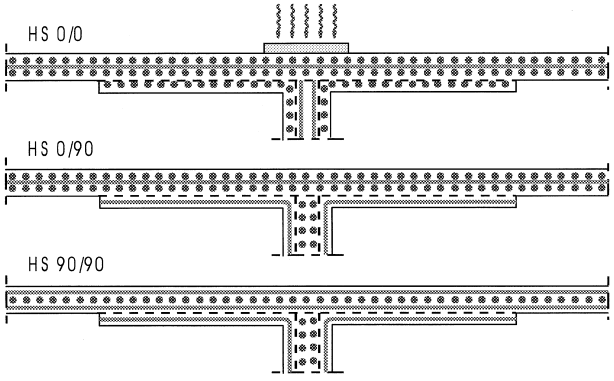

Fig. 5. Stacking sequence of test structures (schematic).

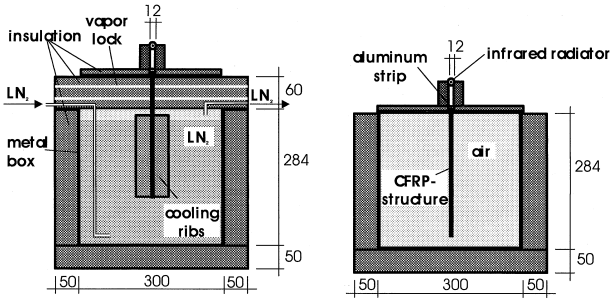

Fig. 6. Test set-up (schematic).

achievable: however, a well-defined initial temperature distribution could be recorded. It was heated until below the lamp the structure had reached a maximum temperature of 130°C. The surface below the radiator was covered by a 5-mm thick aluminum strip, which

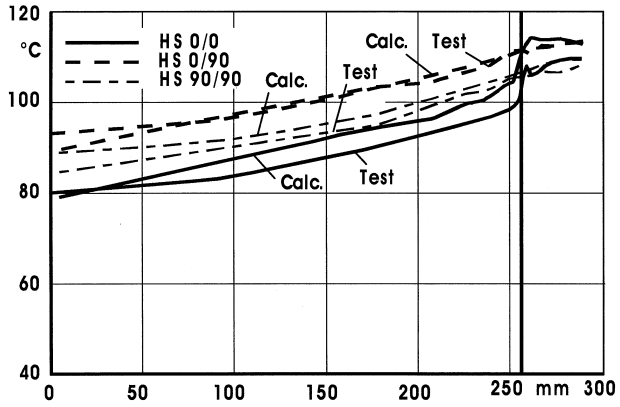

Fig. 7. Temperature distribution along Line B: air cooling.

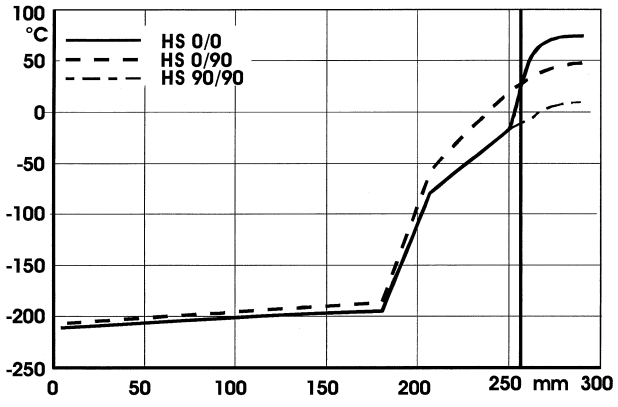

Fig. 9. Temperature distribution along line B: liquid-nitrogen cooling: calculation results.

distributed the heat uniformly. Grooves milled into the bottom side of the strip served for the placing of the thermocouples.

The comparative calculations were carried out by using QUADQL elements. Temperature distributions along line B (see Fig. 4) are depicted in Fig. 7. The agreement between test and calculation is excellent for HS90/90 and good for HS0/0, where a maximum deviation of less than 5°C occurred. It can be seen that the 0° layers within the stiffener root of the structure HS0/0 cause a sharp temperature gradient, which is very well reflected by the finite-element result. All computations could be conducted linearly since the influence of the temperature dependence of the material properties was negligible. Figs. 8 and 9 show the test and calculation results, respectively, for liquid-nitrogen cooling. Non-linear calculations were necessary as a result of the strong temperature dependence of the material properties in the cryogenic temperature range. All computed temperatures are significantly lower than the test results, which is most probably a consequence of the uncertain temperature coefficients (cf. Table 3). That is why only a qualitative comparison can be made. Again, it can be observed that the stacking sequence strongly influences the temperature gradient near the root of the stiffener. The finite element QUADQL is very well suited to reflect this effect, therefore it can be used for the design of thermally-loaded composite structures in order to optimize them w.r.t. thermal stresses caused by temperature gradients.

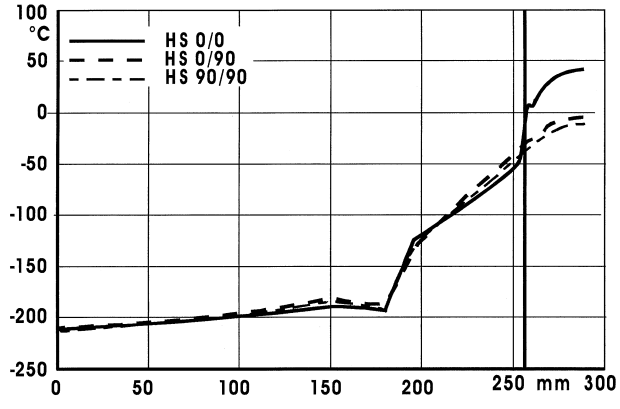

Fig. 8. Temperature distribution along line B: liquid-nitrogen cooling: test results.

3. 3D stresses in layered structures

Plates and shells from multidirectional composite laminates are predominantly designed to carry membrane and bending loads. This holds for relatively slender structures under both thermal and mechanical loads. It is undisputed that 2D theories like the classical thin lamination theory (CLT) or the first order shear deformation theory (FSDT) are in many cases sufficient to determine the in-plane stresses. However, transverse stresses are much more important in layered composites than in metal structures. They can initiate delaminations and, in the case of compression transverse to the fibre direction, failure will occur in a transverse shearing mode which may cause severe damage to adjacent layers.

Various techniques have therefore been proposed for the determination of the transverse stresses in laminated composites. These include 3D or quasi-3D finite elements [13,18,34,35], higher-order 2D theories with either non-linear or piecewise linear approximation of the displacements in the thickness direction [4,8,24] or post-processing techniques used in conjunction with standard 2D analyses. Experience with most of the 3D and higher order 2D approaches has revealed that accurate transverse stresses need relatively high computational effort [4,5,7,11,22]. The use of FSDT is considerably less expensive and, starting from their results, post-processing procedures can determine all transverse stress components. Besides a predictor/corrector approach [16], the use of the equilibrium equations has been rather successful [7,12,17,20]. In general, this requires higher-order shape functions to allow for second derivatives of the in-plane stresses. In

order to relax this deficiency, simplifying assumptions must be introduced. They should reduce the computational effort considerably, whereas the applicability must not be significantly impaired.

Two approximations originally introduced by Rohwer [25] for setting up improved transverse shear stiffnesses have proved quite useful in this respect. Assuming orthogonal cylindrical bending modes relate the bending moment derivatives to the transverse shear forces. If, in addition, the contribution of the in-plane force derivatives to the transverse shear is neglected, then the latter can be directly determined from the local equilibrium in the in-plane directions. They appear as layerwise quadratic functions of the transverse shear forces, temperature distribution and cross-sectional quantities. For plates under mechanical load, this approach yields excellent results, as has been shown by Rolfes and Rohwer [32].

The introduction of these transverse shear stresses into the local transverse equilibrium condition leads to a functional relationship for the transverse normal stress distribution over the laminate thickness. Results for laminated plates under distributed transverse loading obtained by this procedure compare very well with 3D elasticity solutions [33]. Further development along this line includes the effect of thermal loads as well as the application to shell structures [26,31]. With the exception of some special cases under a non-constant thermal load, the accuracy of the approach is surprisingly good.

Because of the extension to allow the determination of transverse stresses from an originally 2D analysis, the method described above is called an 'extended 2D' method. It can be stated that this method calculates the transverse stresses simply by means of first and second derivatives of the shape functions, respectively. That means that standard finite plate and shell elements with quadratic approximation functions are sufficient to determine the transverse stress components in layered composites locally.

4. Integrated analysis process

The interaction of the extended 2D method for 3D thermal and mechanical analysis is demonstrated by the example of a composite wing box. It is assumed that the wing of an aircraft has been heated up on the ground as a result of high solar irradiation. The purpose of the investigation was to simulate how the wing cools down during the starting of the aircraft. Fig. 10 shows the temperature field of the box after 20 s calculated by using four-noded QUADTL elements. They are implemented into the FEM code B2000 [14]. The stress analysis was carried out for the box fixed at the upper and lower edges of one rib after 20 s. In addition to the thermal loads, uniform pressure on the upper and lower surfaces, together with bending moments, were introduced. Eight-noded isoparametric elements were used. For simplicity the meshes were chosen in such a way that four QUADTL elements constituted one stress element. This restriction of the mesh geometry is not necessary if standard pre- and post-processors are used. They allow for interpolating the temperatures between arbitrary meshes as long as they are defined on the same geometry. Fig. 11 gives the displacement field in the y direction. From the output of the FE analyser (T; $T_{,\alpha}$; $T_{,\alpha\beta}$; $\underline{R}$; $\underline{R}_{,\alpha}$) the independently working postprocessor TRAVEST, based on the extended 2D method, provides transverse stress distributions at arbitrary points.

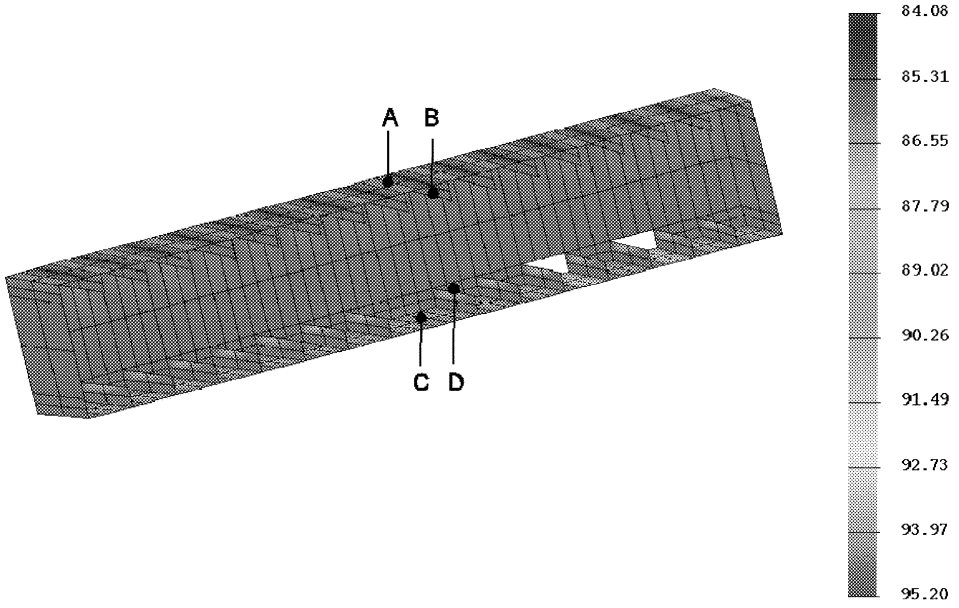

Fig. 10. Temperature distribution on the middle surface of a composite wing box after 20 s.

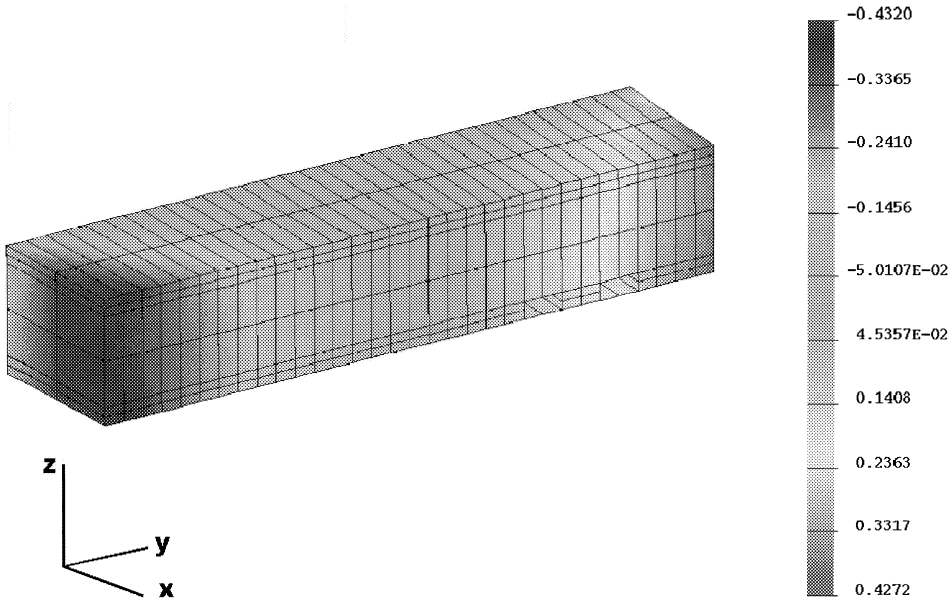

Fig. 11. Displacements in the y direction of a composite wing box under combined thermal and mechanical load.

5. Conclusions and outlook

The main behaviour aspects of relatively thin plates and shells should be describable by 2D models, even if they are set up from layered composites. On the basis of this simple idea, two topics are treated in this paper, thermal behaviour and stress analysis.

It is shown that thermal lamination theories, assuming a linear or quadratic temperature distribution across the thickness, are well suited to capture the 3D temperature field for laminates where the direction of thermal anisotropy changes drastically from layer to layer. Both steady-state and transient problems can be calculated by means of the 2D finite elements QUADTL and QUADQL, which are developed by using the linear and quadratic laminate theories, respectively. In particular, the behaviour of the elements for non-linear problems, either caused by temperature dependence of the material properties or by radiative boundary conditions, is treated. The finite-element results are verified by characteristic tests.

In-plane stresses in laminated structures caused by both thermal and mechanical loads are accurately determined by means of the first-order shear deformation theory. Equilibrium conditions can be applied to calculate the transverse stresses locally. Simplifying assumptions allow us to reduce the order of differentiation of the shape functions so that linear functions suffice to determine transverse shear stresses, whereas quadratic functions are needed for the transverse normal stresses.

The major advantage of the 2D analyses appears when thermal and mechanical problems are to be analysed for the same structure. Its geometrical description can be two-dimensional throughout. Even if different element meshes are needed for the different analysis aspects, the computational effort is relatively small as field interpolation procedures are available in common pre- and postprocessors.

Along the lines of the approach presented, further development with respect to thermal and stress analysis would be useful. Thermal protection systems often consist of several layers with different conductivities in the thickness direction. This leads to a temperature distribution which would need a layerwise approximation. A thermal lamination theory based on that idea is already under development. With respect to the determination of transverse stresses, the applicability of the extended 2D method to sandwich structures should be checked. Furthermore, finite-element users prefer simple elements with linear shape functions. In order to render possible the determination of transverse normal stresses, in this case an additional development is also required. Finally, an extension to doubly-curved shells should be made. Considering the success and the advantages reached so far, these additional steps should be worth the effort.

References

[1] Argyris J, Tenek L. Steady-state nonlinear heat transfer in stiffened composite plates and shells by an exactly integrated facet triangular element. Computer Methods in Applied Mechanics and Engineering 1996;129:53–79.

[2] Argyris J, Tenek L, Öberg F. A multilayer composite triangular element for steady-state conduction/convection/radiation heat transfer in complex shells. Computer Methods in Applied Mechanics and Engineering 1995;120:271–301.

[3] Bose A, Surana KS. Piecewise hierarchical p-version axisymmetric shell element for non-linear heat conduction in laminated composites. Computers & Structures 1993;47:1–18.

[4] Chaudhuri RA. An equilibrium method for prediction of transverse shear stresses in a thick laminated plate. Computers & Structures 1986;23:139–46.
[5] Chaudhuri RA, Seide P. An Approximate semi-analytical method for prediction of interlaminar shear stress in an arbitrarily laminated thick plate. Computers & Structures 1987;25:627–36.
[6] Cuntze RG, Sukarie G. Effective dimensioning of 3D-stressed UD-laminae based on fracture-type strength criteria. In: Tenth International Conference on Mechanics of Composite Materials, Riga, Latvia. Proceedings Institute of Polymer Mechanics, 1998. p.105.
[7] Engblom JJ, Ochoa OO. Through-the-thickness stress predictions for laminated plates of advanced composite materials. International Journal for Numerical Methods in Engineering 1985;21:1759–76.
[8] Gruttmann F, Wagner W. On the numerical analysis of local effects in composite structures. Composite Structures 1994;29:1–12.
[9] Hartwig G, Knaak S. Fibre–epoxy composites at low temperatures. Crogenics 1984;24:639–47.
[10] Hashin Z. Failure criteria for unidirectional fiber composites. Journal of Applied Mechanics 1980;47:329–34.
[11] Kant T, Pandya BN. A simple finite element formulation of a higher-order theory for unsymmetrically laminated composite plates. Composite Structures 1988;9:215–46.
[12] Manjunatha BS, Kant T. On evaluation of transverse stresses in layered symmetric composite and sandwich laminates under flexure. Engineering Computations 1993;10:499–518.
[13] Mau ST, Tong P, Pian THH. Finite Element Solutions for Laminated Thick Plates. Journal of Composite Materials 1972;6:304–11.
[14] Merazzi S. B2000 processors and input description. Switzerland: SMR Engineering & Development, Biel, 1993.
[15] Noor AK, Burton WS. Steady-state heat conduction in multilayered composite plates and shells. Computers & Structures 1991;39:185–93.
[16] Noor AK, Burton WS, Peters JM. Predictor–corrector procedure for stress and free vibration analyses of multilayered composite plates and Shells. Computer Methods in Applied Mechanics and Engineering 1990;82:341–64.
[17] Noor AK, Kim YH, Peters JM. Transverse shear stresses and their sensitivity coefficients in multilayered composite panels. AIAA Journal 1994;32:1259–69.
[18] Owen DRJ, Li ZH. A refined analysis of laminated plates by finite element displacement method — I: fundamentals and static analysis. Computers & Structures 1987;26:907–14.
[19] Padovan J. Steady conduction of heat in linear and nonlinear fully anisotropic media by finite elements. Journal of Heat Transfer 1974;96:313–8.
[20] Pryor CW, Barker RM. A finite element analysis including transverse shear effects for application to laminated plates. AIAA Journal 1971;9:912–7.
[21] Puck A. Festigkeitsanalyse von Faser-Matrix-Laminaten, Modelle für die Praxis. Carl Hanser Verlag: München, Wien, 1996.
[22] Reddy JN, Barbero EJ, Teply JL. A plate bending element based on a generalized laminate plate theory. Internat Journal for Numerical Methods in Engineering 1989;28:2275–92.
[24] Robbins Jr DH, Reddy JN. Modelling of thick composites using a layerwise laminate theory. Internat Journal for Numerical Methods in Engineering 1993;36:655–77.
[25] Rohwer K. Improved transverse shear stiffnesses for layered finite elements. Forschungsbericht DFVLR-FB 88-32, Braunschweig, 1988.
[26] Rohwer K, Rolfes R. Calculating 3D stresses in layered composite plates and shells. Mechanics of Composite Materials 1998;34(4):491–500.
[27] Rolfes R. Efficient thermal analysis of anisotropic composite plates using new finite elements. In: Füller J, Grüninger G, Schulte K, Bunsell AR, Massiah A, editors. Developments in the science and technology of composite materials, Proceedings Fourth European Conference on Composite Materials (ECCM4), Stuttgart, Germany. Elsevier Applied Science, 1990. p. 743–8.
[28] Rolfes R. Higher order theory and finite element for heat conduction in composites. In: Lewis RW, Chin JH, Homsy GM, editors. Numerical methods in thermal problems, Conference Proceedings, Vol. VII, Part 2, Stanford CA, USA. Pinderidge Press, 1991. p. 880–9.
[29] Rolfes R. Nonlinear transient thermal analysis of composite structures. In: Hirsch Ch, Zienkiewicz OC, Onate E, editors. Numerical methods in engineering '92, Conference Proceedings, Brussels, Belgium. Elsevier, 1992. p. 653–9.
[30] Rolfes R, Hammerschmidt U. transverse thermal conductivity of CFRP-laminates: a numerical and experimental validation of approximation formulae. Composites Science and Technology 1995;54:45–54.
[31] Rolfes R, Noor AK, Sparr H. Evaluation of transverse thermal stresses in composite plates based on first-order shear deformation theory. Computer Methods in Applied Mechanics and Engineering 1998;167:355–68.
[32] Rolfes R, Rohwer K. Improved transverse shear stresses in composite finite elements based on first order shear deformation theory. Internat Journal for Numerical Methods in Engineering 1997;40:51–60.
[33] Rolfes R, Rohwer K, Ballerstaedt M. Efficient linear transverse normal stress analysis of layered composite plates. Computers & Structures 1998;68:643–52.
[34] Spilker RL. Hybrid-stress eight-node elements for thin and thick multilayer laminated plates. International Journal for Numerical Methods in Engineering 1982;18:801–28.
[35] Spilker RL, Chou SC, Orringer O. Alternate hybrid-stress elements for analysis of multilayer composite plates. J of Composite Materials 1977;11:51–70.
[36] Surana KS, Orth NJ. Completely hierarchical axisymmetric shell element based on p-version for heat conduction in laminated composites. Computers & Structures 1991;38:429–48.
[37] Tamma KK, Yurko AA. A unified finite element modelling/analysis approach for thermal–structural response in layered composites. Computers & Structures 1988;29:743–54.